Atmospheric Environment 42 (2008) 8371–8381

Contents lists available at ScienceDirect

Atmospheric Environment

journal homepage: www.elsevier.com/locate/atmosenv

An aerodynamic correction for the European ozone risk assessment methodology

Juha-Pekka Tuovinen [a,*], David Simpson [b]

[a] Finnish Meteorological Institute, P.O. Box 503, FI-00101 Helsinki, Finland
[b] Norwegian Meteorological Institute, P.O. Box 43 Blindern, NO-0313 Oslo, Norway

ARTICLE INFO

Article history:
Received 19 May 2008
Received in revised form 12 August 2008
Accepted 13 August 2008

Keywords:
Ozone deposition
Roughness sublayer
Stomatal flux
AOT40
EMEP

ABSTRACT

In Europe the risk of ozone damage to vegetation is assessed using two different metrics, the concentration-based AOT40 index and the flux-based $AF_{st}Y$ index. An important part of the definition of both these indices is that ozone concentrations must be known at the top of the vegetation canopy. An estimate of canopy-top concentrations entails an estimate of the above-canopy concentration gradient, which is affected by the roughness sublayer (RSL) present above an aerodynamically rough surface. A calculation method is derived to correct the aerodynamic resistance for the effect of RSL. This correction results in systematically higher canopy-top concentrations as compared to standard Monin–Obukhov similarity theory. The effect of the modified concentration profile is quantified based on data from the chemical transport model of the European Monitoring and Evaluation Programme, with calculations for crops and forests at six different locations in Europe. Although the average change in ozone concentrations is not very large, the resulting changes in AOT40 and $AF_{st}Y$ metrics can be significant. The RSL leads to increases in AOT40 of 6–13% for forests across the example sites, and 11–24% for crops. $AF_{st}1.6$ only increases by 3–4% for forests, but for crops $AF_{st}6$ increases by 16–54%.

1. Introduction

Ozone is considered one of the most harmful air pollutants affecting human health and vegetation. In Europe, the development of emission control strategies is founded on the effects-based approach, with the ozone-induced plant injury being one of the effects considered (Sliggers and Kakebeeke, 2004). Within this framework, the risk of ozone damage to vegetation is related to numerical exposure and dose metrics (Ashmore et al., 2004; Mills, 2004). These metrics aim at biological meaningfulness, allowing accurate local-scale risk assessment, but are also by design sufficiently uncomplicated to provide 'plausible' regional-scale risk maps based upon a limited amount of data, rather than unjustifiably complex formulations (Hayes et al., 2007; Paoletti and Manning, 2007; Simpson et al., 2007).

The exposure- and dose-type metrics differ in that the former can be evaluated from data on ambient ozone concentrations only, while the latter involves the stomatal uptake of ozone by vegetation and thus, additionally, requires the stomatal conductance of plants to be measured or modelled. Both types of risk indicator are used within the air pollution assessment methodology adopted within the Convention of Long-range Transboundary Air Pollution of the United Nations Economic Commission for Europe (UNECE). This methodology is detailed in a technical guideline document, the so-called Mapping Manual (MM), a major part of which is dedicated to ozone (Mills, 2004). More specifically, the AOTX (Accumulated exposure Over a Threshold of X) exposure index and the $AF_{st}Y$ (Accumulated stomatal flux F_{st} above a threshold of Y) dose index

* Corresponding author. Tel.: +358 919295515; fax: +358 919293503.
E-mail address: juha-pekka.tuovinen@fmi.fi (J.-P. Tuovinen).

1352-2310/$ – see front matter © 2008 Elsevier Ltd. All rights reserved.
doi:10.1016/j.atmosenv.2008.08.008

are defined for ozone in the MM (Mills, 2004). In both cases, the accumulation is to be carried out over the growing season representative of the vegetation in question.

The MM methods have been built into the chemical transport model (CTM) of the European Monitoring and Evaluation Programme (EMEP) (Emberson et al., 2000; Simpson et al., 2003a, 2007). The EMEP model is widely employed within the European air pollution abatement strategy and legislation work (Sliggers and Kakebeeke, 2004; CEC, 2005).

A specific feature common to both the AOTX and A$F_{st}Y$ indices, as adopted within the MM, is that they are explicitly defined in terms of the concentration at the top of the vegetation canopy (Mills, 2004). In any application of these indices, whether based on measurements above the canopy or modelling, it is thus necessary to apply a profile correction, because typically there is a positive, deposition-sink generated vertical concentration gradient above an active vegetation surface. A failure to correct for this gradient will potentially overestimate the risk of ozone-induced damage. The same in principle applies to other exposure indices as well, such as those considered in the United States (Paoletti and Manning, 2007). When AOTX, A$F_{st}Y$ or other similar indices with a concentration or flux threshold are used to assess the risk, even small uncertainties in estimated concentrations can have a larger, nonlinear effect on the risk metrics (Tuovinen, 2000; Sofiev and Tuovinen, 2001; Tuovinen et al., 2007).

Along with an even simpler methodology, consisting of tabulated scaling factors, the MM details equations for calculating the vertical concentration profile from physical principles (Mills, 2004). These are applicable to the atmospheric surface layer in neutral stability conditions, but this approach can be easily enhanced by applying the well-established Monin–Obukhov similarity theory (MOST), if sufficient meteorological data are available. MOST describes the relationship between the vertical flux and mean gradient also in the non-neutral case, that is, when modifying buoyancy forces are present (e.g. Garratt, 1992; Foken, 2006).

An additional complication for the estimation of vertical gradients of scalar quantities, such as trace gas concentrations, arises from the existence of the so-called roughness sublayer (RSL). The RSL is located in the lower part of the surface layer and represents the region immediately above an aerodynamically rough surface, such as a vegetation canopy, in which the traditional flux–gradient relationships of MOST tend to break down (e.g. Garratt, 1992). This has been observed for various vegetation types including pine forests (Thom et al., 1975; Raupach, 1979; Högström et al., 1989; Rannik, 1998), a mixed pine–spruce forest (Mölder et al., 1999), mixed coniferous–deciduous forests (Bosveld, 1997; Neirynck et al., 2005), a mixed pine–oak forest (Schween et al., 1997), savannah forests (Garratt, 1980), an aspen forest (Nakamura and Mahrt, 2001), a mixed aspen–maple forest (Simpson et al., 1998), beech forests (Dellwik and Jensen, 2005; Mammarella et al., 2008), bushland (Chen Fazu and Schwerdtfeger, 1989), a sugar cane field (Cellier, 1986) and a maize field (Cellier and Brunet, 1992). Observations suggest that the RSL extends from the vegetation canopy height (h) to approximately $2h$.

The studies listed above do not explicitly consider trace gas concentration profiles but provide quite a consistent picture of the deviations of RSL from the traditional MOST that is applicable to any scalar. In simple terms, while the time-averaged vertical turbulent fluxes of energy and mass remain approximately constant with height in the surface layer, in the RSL the corresponding eddy diffusivities are enhanced due to the direct influence of roughness elements on the flow. Correspondingly, the vertical gradients of different scalars are reduced in the RSL. This affects the near-surface concentrations that are derived using the flux–gradient relationship, the traditional MOST in principle resulting in an underestimated concentration, if applied within the RSL.

The importance of the MOST-based profile correction for near-surface concentrations has been demonstrated earlier (Tuovinen, 2000) and, as explained above, is acknowledged in the MM (Mills, 2004). Even though the uncertainty related to the RSL is recognised in the MM, no guidance is provided for dealing with the problem. Obviously, the MM methodology and the related European-scale risk assessments can never aim to cope with all the uncertainties associated with predicting the above-canopy ozone concentrations and fluxes, including those traditionally involved in biosphere–atmosphere studies (e.g. Raupach, 1995). These difficulties are exacerbated by the complexity and variability of the natural systems to be studied and mapped, and further compounded when trying to make assessments over large areas such as for the whole of Europe (e.g. Erisman et al., 2005). It is important, however, that the possible sources of uncertainty are identified and quantified as far as possible.

In the present work we derive a simple calculation method for estimating the influence of RSL on the canopy-top concentration, and further on the exposure and dose indices. The method is applied here in the context of the EMEP CTM, but is not limited to this particular model; it can be used for measured ozone concentration data as well. By employing model-derived ozone concentrations and fluxes and related meteorological data for different geographical locations and vegetation types in Europe, we quantify and assess the importance of this RSL correction for the AOTX and A$F_{st}Y$ indices. Finally, we discuss the uncertainties related to the suggested method.

2. Material and methods

2.1. Deposition parameterisation

Within the EMEP model, as in most Eulerian CTMs, the dry deposition fluxes are calculated as a vertical boundary condition of the equations describing the dynamics of atmospheric processes (Simpson et al., 2003a,b). The mass flux density of ozone (Q_c, positive away from the surface) is expressed as being proportional to the dry deposition velocity (V_d),

$$Q_c = -V_d(z)c(z) \quad (1)$$

where c is ozone concentration and z is the height above the ground. The dry deposition velocity is parameterised as

$$V_d(z) = \frac{1}{R_a(z_0+d,z)+R_b+R_s} \quad (2)$$

where $R_a(z_1, z_2)$ denotes the aerodynamic resistance between the heights z_1 and z_2, z_0 is the roughness length of momentum, d is zero-plane displacement, R_b is the canopy-scale quasi-laminar resistance and R_s is the canopy-scale surface resistance.

The aerodynamic resistance is calculated from

$$R_a(z_1,z_2) = \frac{1}{\kappa u_*}\left(\ln\frac{z_2-d}{z_1-d} - \Psi(\zeta_1,\zeta_2)\right) \quad (3)$$

where κ ($=0.4$) is the von Kármán constant and u_* is friction velocity; Ψ is the diabatic influence function of MOST, which only depends on the dimensionless stability parameter $\zeta_i \equiv (z_i-d)/L$ ($i = 1,2$); L is the Obukhov length [$L = -\theta_v u_*^3/\kappa g Q_{\theta_v}$, where θ_v is the virtual potential temperature, g ($=9.8\ \mathrm{m\,s^{-2}}$) is the acceleration due to gravity and Q_{θ_v} is the kinematic buoyancy flux density]. We assume that the Ψ function determined for sensible heat is applicable to ozone transfer. The detailed equations are presented in Appendix.

For the quasi-laminar resistance, the formula suggested by Hicks et al. (1987) is used in the EMEP model. The total surface resistance R_s consists of stomatal and non-stomatal components, which are modelled as a function of environmental and plant phenological factors (Emberson et al., 2000; Simpson et al., 2003a; Tuovinen et al., 2004). The exact form of functions and parameters needed for R_s varies with different vegetation types, and it has been accepted that for integrated assessment modelling some simple 'generic' vegetation classes can be defined (Simpson and Emberson, 2006). These generic classes represent a mixture of real plant species, with detailed temperature, light and humidity response functions, but strongly simplified phenology. Parameter values for the environmental functions were updated to those recommended for large-scale modelling in the revised version of the MM (Mills, 2007). In this work we consider two different vegetation canopy types included in the EMEP model, the so-called generic crop (with characteristics based largely upon wheat data) and generic deciduous forest (based largely upon beech) (Simpson and Emberson, 2006), which are parameterised in addition to the standard land cover classes (LCCs) (Simpson et al., 2003a).

Following Mills (2007), the vegetation height is set to $h = 1$ m and 20 m for the generic crop and forest, respectively, and it is assumed that $z_0 = 0.1h$ and $d = 0.7h$. The assumption of a fixed crop height, and indeed of using simplified extended growing seasons, is made because of the difficulties of knowing the real phenology of different vegetation types across Europe and the variation within large grid elements (Mills, 2007; Simpson and Emberson, 2006). In the calculations based on the EMEP model data, the reference height (z_r) is set to 45 m, which is approximately the height of the lowest vertical grid point of the model and is assumed to be located within the surface layer.

2.2. Data

The effect of the RSL correction was analysed using hourly data for six grid elements of the EMEP model (Table 1), extracted from the European-scale fields of meteorological, concentration and deposition data for the year 2000 (thus containing both input and output data of the model). The meteorological input data are based on a dedicated version of the operational HIRLAM (High Resolution Limited Area Model) numerical weather prediction model; for details, see Benedictow (2003) and Simpson et al. (2003a).

The horizontal resolution of the EMEP model is about 50 km × 50 km. Within each grid element, the differences in surface characteristics between LCCs are taken into account in the parameterisation of the surface resistance. In addition, the HIRLAM-based grid-element average u_* is adjusted for each LCC according to the local momentum roughness length (Simpson et al., 2003a,b). This results in a higher u_* for rough surfaces and thus in different u_* and L values for the two vegetation types considered here.

The six EMEP grid elements selected for this study cover different climatic and air quality conditions. The same modelled data set has been used in a robustness analysis of the AOTX and AF$_{st}Y$ indices by Tuovinen et al. (2007), who also made use of measured ozone concentration data. Even though the present study involves no direct measurement data, for convenience the location of the grid elements is denoted by an EMEP measurement site located within each element (Hjellbrekke and Solberg, 2002) (Table 1).

2.3. Exposure and dose indices

Within the MM ozone risk assessment methodology of UNECE (Mills, 2004), the AOTX exposure and AF$_{st}Y$ dose indices are defined as

Table 1
EMEP measurement sites representing the location of input data and the corresponding accumulation periods for the exposure and dose indices

Station	Country	EMEP code	Location	Accumulation period		
				Crop		Forest
				AOTX	AF$_{st}Y$	
Rörvik	Sweden	SE02	57°25′ N, 11°56′ E	1/6–31/8	21/6–14/8	1/4–30/9
Eskdalemuir	UK	GB02	55°19′ N, 3°12′ W	1/5–31/7	16/6–9/8	1/4–30/9
Langenbrügge	Germany	DE02	52°48′ N, 10°46′ E	15/4–15/7	9/6–2/8	1/4–30/9
Stará Lesná	Slovakia	SK04	49°09′ N, 20°17′ E	15/4–15/7	31/5–24/7	1/4–30/9
Ispra	Italy	IT04	45°48′ N, 8°38′ E	1/4–30/6	22/5–15/7	1/4–30/9
Campisabalos	Spain	ES09	41°17′ N, 3°09′ W	1/4–30/6	11/5–4/7	1/4–30/9

$$\mathrm{AOT}X = \sum_{i=1}^{N} \max(c_i(h) - X, 0)\Delta t \quad (4)$$

and

$$\mathrm{AF_{st}}Y = \sum_{i=1}^{M} \max(F_{\mathrm{st},i} - Y, 0)\Delta t \quad (5)$$

where X is the threshold concentration (in ppb or nl $\mathrm{l^{-1}}$), F_{st} is the stomatal ozone flux per projected leaf area (PLA) to sunlit leaves at the canopy top and Y is the threshold stomatal flux per PLA (in nmol $\mathrm{m^{-2}\,s^{-1}}$). The calculation of AOTX and AF$_{\mathrm{st}}Y$ is based on hourly values (denoted by i), so $\Delta t = 1$ h; N and M denote the number of hours to be included in the calculation period (daylight hours only). The accumulation period corresponds to the observed or assumed growing season. The periods used in this study are based on the MM recommendations (Mills, 2004) and are shown in Table 1.

We consider the AF$_{\mathrm{st}}$6 and AF$_{\mathrm{st}}$1.6 indices, based on which the so-called critical levels of ozone are defined for crops and forests, respectively (Mills, 2004). The exposure-based critical levels are expressed as AOT40 for both. In addition, we calculated AF$_{\mathrm{st}}$0 (no threshold, i.e. the total dose) for both vegetation types and AF$_{\mathrm{st}}$3 for the generic crop, the latter of which is defined for integrated assessment applications for its higher degree of robustness (Simpson and Emberson, 2006; Tuovinen et al., 2007).

3. Results and discussion

3.1. Calculation of the canopy-top concentration

According to MOST, the vertical fluxes of momentum and passive scalars remain approximately constant with height within the atmospheric surface layer (e.g. Garratt, 1992). To derive the relationship between the ozone concentration at the top of the canopy and that determined (measured or modelled) at a higher level within the surface layer (here at the model reference level z_{r}), we express the MOST-based aerodynamic resistance between heights z_1 and z_2 as

$$R_{\mathrm{a}}(z_1, z_2) = \frac{c(z_1) - c(z_2)}{Q_c}, \quad z_1 \le z_2 \quad (6)$$

and the corresponding aerodynamic resistance within the RSL that has been corrected for the enhanced eddy diffusivity as

$$R^*_{\mathrm{a}}(z_1, z_2) = \frac{c^*(z_1) - c^*(z_2)}{Q_c}, \quad z_1 \le z_2 \le z^* \quad (7)$$

where c^* is the actual (corrected) concentration within the RSL and z^* is the RSL height. Here we assume $z^* = 2h$ and explore an uncertainty range of $z^* = 1.5h$–$2.5h$.

Within this framework, $c(z)$ does not represent the actual concentration for $z < z^*$, but an extrapolation of the MOST-based profile down into the RSL. By evaluating Eq. (1) at $z = z_{\mathrm{r}}$, utilizing $c(z^*) = c^*(z^*)$ and setting $z_1 = z^*$ and $z_2 = z_{\mathrm{r}}$ in Eq. (6), and $z_1 = h$ and $z_2 = z^*$ in Eq. (7), we obtain the RSL-corrected canopy-top concentration:

$$c^*(h) = \left[1 - \left(R^*_{\mathrm{a}}(h, z^*) + R_{\mathrm{a}}(z^*, z_{\mathrm{r}})\right) V_{\mathrm{d}}(z_{\mathrm{r}})\right] c(z_{\mathrm{r}}), \quad h \le z^* \le z_{\mathrm{r}} \quad (8)$$

In situations in which the reference height is within the RSL, we can write

$$c^*(h) = \left[1 - R^*_{\mathrm{a}}(h, z_{\mathrm{r}}) V_{\mathrm{d}}(z_{\mathrm{r}})\right] c(z_{\mathrm{r}}), \quad h \le z_{\mathrm{r}} \le z^* \quad (9)$$

Eqs. (8) and (9) are basically similar to the corresponding equation derived from the standard EMEP model version (cf. Tuovinen et al., 2007), with the exception of the aerodynamic resistance between h and z_{r} [i.e. $R^*_{\mathrm{a}}(h, z^*) + R_{\mathrm{a}}(z^*, z_{\mathrm{r}})$ or $R^*_{\mathrm{a}}(h, z_{\mathrm{r}})$ instead of $R_{\mathrm{a}}(h, z_{\mathrm{r}})$].

Analogously to Eq. (3), the RSL-corrected aerodynamic resistance can be written as

$$R^*_{\mathrm{a}}(z_1, z_2) = \frac{1}{\kappa u_*}\left(\ln\frac{z_2 - d}{z_1 - d} - \Psi^*(\zeta_1, \zeta_2)\right) \quad (10)$$

where the Ψ^* function represents the combined influence of stability and RSL. A detailed derivation of R^*_{a} and Ψ^* is presented in Appendix.

It is worth noticing that the parameterisation of V_{d} [Eq. (2)] involves an aerodynamic resistance between the surface and a reference level above. By definition, this is the MOST-based form [Eq. (3)], which within the RSL is extrapolated down to $z = z_0 + d$, instead of applying R^*_{a} to $z < z^*$. With the extrapolated $c(z)$ this formulation is consistent with the assumed constancy of vertical fluxes throughout the surface layer.

3.2. Numerical examples

The RSL correction derived above results in a reduction of the aerodynamic resistance between h and z_{r} (Fig. 1). There is a substantial difference between the corrected and uncorrected resistances, especially in unstable conditions and for larger RSL heights. For the taller vegetation, the resistances also differ in stable conditions. The difference between crop and forest is in this example only due to the different canopy heights, resulting in different depths of

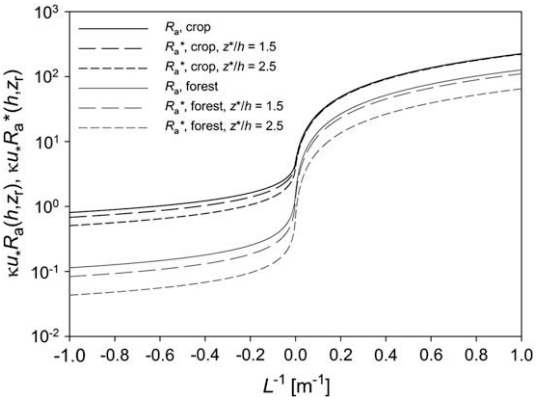

Fig. 1. Dimensionless aerodynamic resistances between the canopy height h (1 m for crop, 20 m for forest) and the reference height $z_{\mathrm{r}} = 45$ m as a function of the inverse Obukhov length.

the layer over which the aerodynamic resistance is integrated; for R_a^*, h also affects z^*, as shown in Appendix.

As explained in Section 2.2, the u_* and L data used within the EMEP model for deposition parameterisations are adjusted to the local, LCC-specific momentum roughness length. This also affects the aerodynamic resistances to some extent. The effect of this adjustment is included in the results presented in Fig. 2, which shows a site-specific example of the RSL-corrected aerodynamic resistance calculated from the EMEP data according to the formulation derived above. The basic pattern and difference between the surface types are similar to Fig. 1, but there is scatter around the stability dependence, because here u_* acts as an additional variable.

Fig. 3 shows examples of modelled vertical concentration profiles. Due to the deposition sink at the surface, ozone concentrations are progressively reduced with reducing height from the value at a reference level, irrespective of whether the influence of RSL is modelled or not. As mentioned above, it is because of this phenomenon that the current definitions of the AOTX and AF$_{st}Y$ indices explicitly refer to the canopy height (Tuovinen, 2000; Mills, 2004).

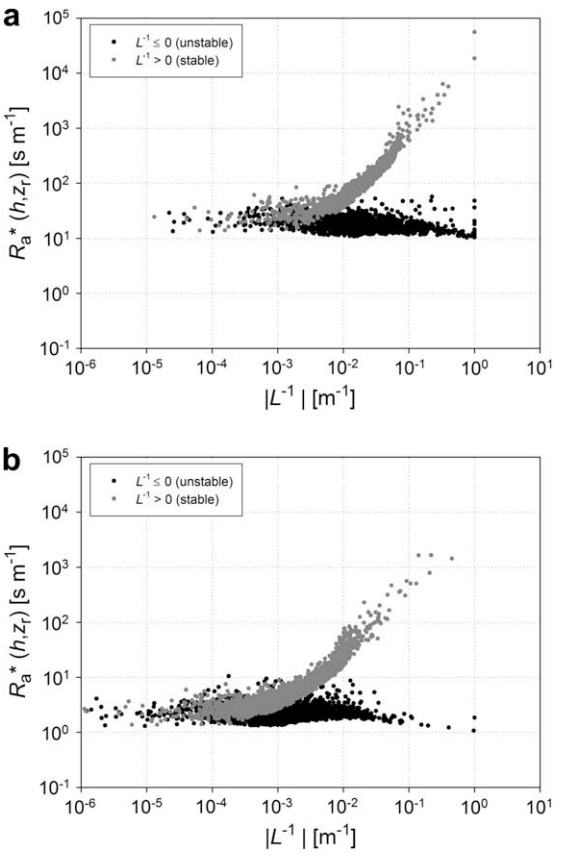

Fig. 2. RSL-corrected aerodynamic resistance between the canopy height h and the reference height $z_r = 45$ m as a function of the inverse Obukhov length, calculated from the EMEP model data with $z^*/h = 2$ for the DE02 grid element (Table 1), for (a) crop ($h = 1$ m) and (b) forest ($h = 20$ m). The data are for the assumed growing seasons of 2000.

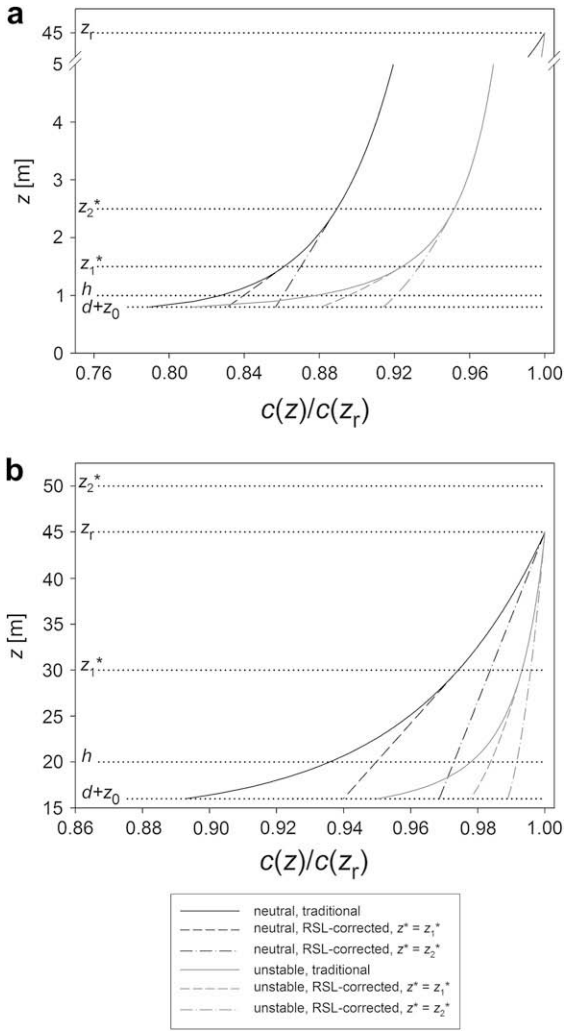

Fig. 3. Vertical ozone concentration profiles for neutral ($u_* = 0.5$ m s^{-1}, $L^{-1} = 0$) and unstable ($u_* = 0.2$ m s^{-1}, $L^{-1} = -0.2$ m^{-1}) conditions with $R_s = 100$ s m^{-1}. The profiles are scaled with respect to the concentration at $z_r = 45$ m and calculated for (a) crop ($h = 1$ m) and (b) forest ($h = 20$ m), and for two different RSL heights, $z_1^* = 1.5h$ and $z_2^* = 2.5h$.

The steepness of the profile depends on atmospheric stability, the canopy-top concentration decreasing with increasing stability. Conditions of stable stratification, not considered in Fig. 3, typically occur at night, when both the stomatal conductance and ozone concentration are generally reduced, and thus these periods can be expected to play a minor role in the context of the present study. The concentration gradient also depends on the surface resistance, which in these example calculations is kept constant at 100 s m^{-1}; lowering the resistance results in a lower canopy-top concentration, and vice versa. Further examples on the effect of stability and surface resistance on the near-surface ozone concentrations, as derived from the traditional MOST, have been presented by Tuovinen (2000).

By definition, the profiles calculated using MOST are identical to the RSL-corrected profiles for $z \ge z^*$ (Fig. 3). As mentioned above, below z^* the MOST-based profiles must

be considered extrapolations beyond the domain of their validity, and the RSL-corrected profiles deviate from them for $z < z^*$. The reduced aerodynamic resistance (Fig. 1) results in significantly higher concentrations at heights close to the top of canopy. In neutral conditions, the RSL correction transforms the logarithmic concentration profile obtained from MOST into a linear profile (Fig. 3). For the taller vegetation, the profile effect (i.e. the concentration reduction from $z_r = 45$ m to $h = 20$ m in this case) is then reduced from 6.4% to 2.7–5.0% (for the assumed range of $z^*/h = 1.5$–2.5), that is, by 22–58%. In the unstable conditions prescribed in the example, the corresponding reduction is from 2.2% to 0.8–1.6% (by 27–62%).

For the shorter vegetation with $h = 1$ m, the profile effect is greater (7.9–17.3%, depending on the treatment of RSL), but the relative influence of RSL on it is weaker (reduction by 7–19% and 14–35% for $z^*/h = 1.5$–2.5 in neutral and unstable conditions, respectively). However, it can be shown that the relative increase in the canopy-top concentration [or $c^*(h)/c(h)$] due to the RSL correction is in unstable conditions larger for the shorter vegetation (also in neutral stability, if $z^* > z_r$ for the taller vegetation; equal relative increase, if $z^* \leq z_r$ for both vegetation heights). It should be noted that the same u_*, L and R_s were assumed for the different vegetation types in this illustrative example.

3.3. Exposure and dose indices

The effect of the RSL correction on the canopy-top concentration is obviously transferred into the AOTX exposure and AF$_{st}Y$ dose indices that are defined in terms of this concentration; however, the outcome of this varies in a nonlinear manner depending on the index type, threshold value and site location. Tables 2–4 show that there is a significant increase in the AOT40 values for both crop (11–24%) and forest (6–13%) and in some, but not all, values of the flux indices (1–54%) calculated for the six EMEP grid elements. In particular, the AF$_{st}$6 index, which is used for the current critical level for crops (Mills, 2004), is strongly influenced by the RSL correction, especially at the Swedish site SE02. It should be noted, however, that this site had the lowest AF$_{st}$6 value to start with and, in terms of absolute change or estimated risk, the increase is much larger at the central and southern European sites. The corresponding index for forest (AF$_{st}$1.6) is rather insensitive (<5%) to the change induced to the canopy-top concentration. The AF$_{st}$3 metric defined for integrated assessment modelling exhibits moderate sensitivity (10–17%).

Clearly, the crop indices are more affected than the forest ones (Tables 2–4). This is related to both the deposition parameterisation and mathematical properties of the indices. The differences largely result from the greater enhancement of the canopy-top concentration due to the RSL correction for shorter vegetation in unstable conditions, but is also affected by different R_s, and the LCC-adjustment of u_* and L. These differences are enhanced when increasing the threshold value, which is a fundamental property of the exposure and dose indices involving a threshold (Tuovinen, 2000; Sofiev and Tuovinen, 2001). The increasing sensitivity explains the differences in the effect of the RSL correction on AF$_{st}Y$ between different threshold values Y, for both the crop and forest data. Furthermore, Tuovinen et al. (2007) demonstrated how the characteristics of the frequency distributions of the stomatal fluxes contributing to AF$_{st}$6 for crop and AF$_{st}$1.6 for forest affect the sensitivity. The higher sensitivity of AF$_{st}$6 originates from the fact that for forest a much higher proportion of the stomatal fluxes exceeds the threshold value of 1.6 nmol m^{-2} s^{-1} than for crop exceeds the threshold of 6 nmol m^{-2} s^{-1}.

3.4. Uncertainties

The aerodynamic correction for the ozone risk assessment methodology derived and analysed above is based on a straightforward application of MOST, with a simple modification for the RSL effects. The fundamental assumptions of MOST are that the atmospheric flow is turbulent and stationary, chemical reactions can be ignored, and that there is no advection and the surface below is horizontally homogeneous (e.g. Garratt, 1992). Obviously, these conditions are not perfectly met in practice, and therefore, the related uncertainties involve most micrometeorological studies. In the following, we briefly discuss these (and some other) problems, as related to the present topic.

3.4.1. Applicability of MOST

Williams et al. (2007) identify two reasons why the applicability of MOST may be weakened in the RSL, namely, (1) departure of turbulence statistics from the universal

Table 2
Values of the AOT40 indices in 2000 as calculated without (traditional) and with (corrected) roughness sublayer effects

Station	AOT40, crop (ppb h)			AOT40, forest (ppb h)		
	Traditional	Corrected		Traditional	Corrected	
		$z^*/h = 2$ (1.5–2.5)[a]	Change[b]		$z^*/h = 2$ (1.5–2.5)[a]	Change[b]
SE02	1526	1764 (1640–1872)	238 (15.6%)	7736	8710 (8217–9084)	974 (12.6%)
GB02	1803	2097 (1946–2222)	294 (16.3%)	5317	5838 (5584–6023)	521 (9.8%)
DE02	6924	7715 (7322–8020)	792 (11.4%)	16809	17912 (17385–18286)	1103 (6.6%)
SK04	5125	6343 (5747–6795)	1218 (23.8%)	20035	21584 (20841–22119)	1549 (7.7%)
IT04	10261	11717 (11037–12206)	1456 (14.2%)	32382	34281 (33382–34928)	1899 (5.9%)
ES09	5473	6592 (6049–6998)	1119 (20.4%)	17095	18102 (17621–18445)	1007 (5.9%)

[a] Assumed uncertainty range.
[b] Increase due to the correction for $z^*/h = 2$.

Table 3
Values of the $AF_{st}Y$ indices for generic crop in 2000 as calculated without (traditional) and with (corrected) roughness sublayer effects

Station	$AF_{st}0$ (mmol m^{-2})			$AF_{st}3$ (mmol m^{-2})			$AF_{st}6$ (mmol m^{-2})		
	Traditional	Corrected		Traditional	Corrected		Traditional	Corrected	
		$z^*/h = 2$ (1.5–2.5)[a]	Change[b]		$z^*/h = 2$ (1.5–2.5)[a]	Change[b]		$z^*/h = 2$ (1.5–2.5)[a]	Change[b]
SE02	10.22	10.79 (10.51–11.00)	0.57 (5.5%)	2.58	3.00 (2.79–3.17)	0.42 (16.5%)	0.28	0.43 (0.36–0.50)	0.15 (54.3%)
GB02	9.85	10.30 (10.09–10.46)	0.46 (4.7%)	3.60	4.01 (3.81–4.15)	0.41 (11.3%)	0.88	1.08 (0.98–1.15)	0.20 (22.5%)
DE02	14.63	15.39 (15.03–15.66)	0.76 (5.2%)	6.85	7.57 (7.22–7.83)	0.72 (10.5%)	2.25	2.74 (2.50–2.92)	0.49 (21.7%)
SK04	11.80	12.46 (12.15–12.69)	0.66 (5.6%)	5.67	6.28 (5.99–6.50)	0.61 (10.8%)	1.93	2.41 (2.18–2.58)	0.48 (24.7%)
IT04	17.24	18.28 (17.79–18.62)	1.03 (6.0%)	10.11	11.08 (10.63–11.41)	0.97 (9.6%)	5.21	6.03 (5.64–6.30)	0.82 (15.8%)
ES09	9.49	10.06 (9.79–10.26)	0.57 (6.0%)	5.05	5.59 (5.33–5.78)	0.55 (10.8%)	1.87	2.32 (2.11–2.48)	0.45 (24.0%)

[a] Assumed uncertainty range.
[b] Increase due to the correction for $z^*/h = 2$.

MOST forms (nonuniversal behaviour) and (2) inequality of these statistics between different scalars (scalar dissimilarity). Both are related to surface heterogeneity; the former may result from the heterogeneity in the source/sink distribution within the vegetation, while the differences between the source/sink distributions of different scalars may induce dissimilarity.

We have addressed the deviation from the universal MOST flux–gradient relationships by modifying the eddy diffusivity in the RSL. While this modification must be perceived as a semi-empirical correction, as compared to the more fundamental MOST, and it is questionable whether the revised flux–gradient function can be considered truly universal, there exists experimental support for this specific form of correction, both for crop (Cellier and Brunet, 1992) and forest surfaces (Mölder et al., 1999).

Above the RSL, similar transport of different passive scalars can be formally expected on the basis of MOST (Hill, 1989; Dias and Brutsaert, 1996). In practice, it is generally assumed that sensible heat and water vapour exhibit similar behaviour over homogeneous surfaces, for example for the commonly-used energy balance/Bowen ratio method of calculating sensible and latent heat fluxes (e.g. Brutsaert, 1982). There is also experimental evidence to support near-perfect similarity between sensible heat and water vapour (Dias and Brutsaert, 1996). However, the agreement may vary within the diurnal cycle of fluxes, even over short vegetation, within which sinks and sources are located close together (Ruppert et al., 2006). Over heterogeneous surfaces or within the RSL, scalar similarity may appear less perfect and has been observed to be influenced by soil moisture (Lamaud and Irvine, 2006) and senescence (Williams et al., 2007), for example.

Specific to the present study is the fact that we are dealing with ozone, for which we have assumed the universal flux–gradient relationships of sensible heat to be applicable. However, the source/sink distribution of ozone may differ from that of heat, especially if affected by chemical reactions taking place inside the canopy (e.g. Dorsey et al., 2004; Goldstein et al., 2004). The similarity issue, even in terms of the traditional MOST, has been addressed in only a few studies on ozone fluxes. Droppo (1985) demonstrated a close correspondence between the eddy diffusivities of ozone and sensible heat (rather than

Table 4
Values of the $AF_{st}Y$ indices for generic forest in 2000 as calculated without (traditional) and with (corrected) roughness sublayer effects

Station	$AF_{st}0$ (mmol m^{-2})			$AF_{st}1.6$ (mmol m^{-2})		
	Traditional	Corrected		Traditional	Corrected	
		$z^*/h = 2$ (1.5–2.5)[a]	Change[b]		$z^*/h = 2$ (1.5–2.5)[a]	Change[b]
SE02	26.20	26.75 (26.48–26.95)	0.55 (2.1%)	11.94	12.46 (12.20–12.65)	0.52 (4.4%)
GB02	24.44	24.80 (24.63–24.92)	0.35 (1.4%)	10.63	10.95 (10.80–11.07)	0.33 (3.1%)
DE02	27.94	28.40 (28.18–28.55)	0.45 (1.6%)	13.96	14.40 (14.19–14.55)	0.44 (3.1%)
SK04	26.09	26.57 (26.34–26.74)	0.49 (1.9%)	12.62	13.08 (12.86–13.24)	0.46 (3.7%)
IT04	33.11	33.88 (33.50–34.15)	0.77 (2.3%)	19.31	20.04 (19.69–20.30)	0.73 (3.8%)
ES09	21.84	22.17 (22.01–22.29)	0.33 (1.5%)	8.79	9.10 (8.95–9.20)	0.31 (3.5%)

[a] Assumed uncertainty range.
[b] Increase due to the correction for $z^*/h = 2$.

momentum) over grassland in unstable conditions. Wesely (1988) observed high negative spectral correlation coefficients between water vapour and ozone concentration fluctuations above a soybean field, indicating similarity of transfer mechanisms. Wesely (1988) also concluded that the normalised standard deviations followed a common power law dependence on stability; the same result was reported by Affre et al. (1999).

Pearson et al. (1998) investigated scalar similarity above a cotton field on the basis of power spectra. The spectra of temperature, humidity and ozone concentration closely followed the expected frequency dependence and agreed with each other well, based on which it was concluded that ozone obeys the scalar similarity relationships in unstable conditions. However, Wesely (1988) and Pearson et al. (1998) did not consider low-frequency (<0.01 Hz) fluctuations, to which Ruppert et al. (2006) could attribute the dissimilarities they observed between temperature, water vapour and carbon dioxide. Investigating a rather limited data set for a coniferous forest, Duyzer and Weststrate (1995) found no significant difference between the RSL-corrected flux–gradient functions for sensible heat and ozone.

In summary, we acknowledge the uncertainties related to the issues of nonuniversal behaviour in the RSL and scalar similarity in general, but argue that the proposed formulation is in fair balance with the present understanding, given the framework of application.

3.4.2. Extent of RSL

One potential uncertainty source within the RSL correction suggested in the present study is that we have assumed the RSL height to be proportional to the canopy height. In some studies it has been observed that z^* could be related to a length scale characterising the main source of horizontal inhomogeneities of the canopy (Garratt, 1980; Cellier, 1986; Cellier and Brunet, 1992; Nakamura and Mahrt, 2001). In forests, this would be the mean spacing between the trees, while for crops the inter-row spacing would provide a more appropriate scale. Verhoef et al. (1997) suggested that z^* should be related to the vertical length scale $u(h)/(\partial u/\partial z)_{z=h}$, where u is wind speed, describing turbulence characteristics within and just above the canopy (Raupach et al., 1996). However, as the vegetation information in the EMEP model is limited to the LCC-specific h and leaf area index, and the meteorological data has a rather coarse resolution, we opted for the simplest alternative.

The proportionality factor $z^*/h = 2$ chosen here is supported by observations for crops by Cellier and Brunet (1992) with $z^*/h \approx 2.2$, and for forests by Mölder et al. (1999) with $z^*/h \approx 2.3$ and Bosveld (1997) with $z^*/h \approx 2.2$. From Rannik et al. (2004), it can be deduced that $z^*/h \leq 2.4$ for a coniferous forest, while the data of Nakamura and Mahrt (2001) imply that $z^*/h = 2.0$–2.5 for a deciduous forest, and those of Simpson et al. (1998) correspond to a similar value. Tables 2–4 provide an indication of the uncertainties related to the value of z^*/h.

3.4.3. Other profiles

In principle, a similar, though not identical, RSL correction should be applied to the wind speed profile as well. Within the risk assessment methodology discussed here, the wind speed at the canopy top must be known for the leaf-scale laminar resistance when calculating the stomatal flux for $AF_{st}Y$ (but is not needed for AOTX) (Mills, 2004). However, this resistance typically does not play an important role and, being proportional to $u(h)^{-1/2}$ (Mills, 2004; Simpson et al., 2007), it can be shown to be rather insensitive to u. Therefore, the RSL correction for wind speed can be expected to have only a minor influence on the model results.

Profiles of water vapour and temperature are also affected by the RSL, and this would have an effect on ozone concentrations and fluxes via stomatal conductance changes. However, this type of feedback entails much smaller changes than the direct effect of RSL on the ozone profile itself, and thus can be ignored within our application.

4. Summary and conclusions

In Europe the risk of ozone damage to vegetation is assessed using two different metrics, the concentration-based AOT40 index and the flux-based $AF_{st}Y$ index. Both metrics have been defined in the so-called Mapping Manual of UNECE. An important part of the definition of both AOT40 and $AF_{st}Y$ is that concentrations of ozone have to be determined at the top of the canopy. Model calculations of ozone, or indeed measurements of ozone concentrations, are typically available at a different (usually higher) reference height, so an estimate of canopy-top concentrations entails an estimate of the vertical concentration gradients between the canopy-top and reference heights. Where available meteorological data allow, this gradient has previously been calculated using standard Monin–Obukhov similarity theory.

The assessment of risks using the MM methodology is obviously fraught with uncertainties, both in biological and physical factors. The biological basis has serious limitations for even real species, and more so for the generic species defined in the MM. However, it is important to assess any uncertainties related to the present MM methods, in order that the correct decisions are taken as to which processes should be included in future formulations. In this context, we have examined the effect of one neglected factor, that of the roughness sublayer, which modifies the vertical concentration profiles. We have presented a method for incorporating RSL effects into AOT40 and $AF_{st}Y$ assessments on local and European scales, and explored the resulting changes for six sites in different pollution/climate locations.

The effect of the correction is to systematically increase the estimated canopy-top concentrations at all sites. Although the change in ozone concentrations is not very large on average, the resulting changes in the AOT40 and $AF_{st}Y$ metrics are much more significant, especially for crops. The values of AOT40 were increased by 6–24%. As a result of the high flux threshold value in $AF_{st}6$ for crop, this statistic is particularly sensitive to the RSL correction, with increases of typically 20% and maximally larger than 50%. For $AF_{st}1.6$ for forest, the increase is rather insignificant (<5%).

The methodology proposed here represents an increase in complication compared to using standard MOST profiles,

but the formulation is rather straightforward and is readily implemented for either chemical transport models or interpretation of measurements. For forests the RSL correction would have only a modest effect on risk metrics, but for crops the correction could be substantial, and may be worth considering if more realistic risk estimates are sought.

Acknowledgements

This work was supported by the ACCENT-BIAFLUX Exchange-of-Staff Programme and for DS by the EMEP project under UNECE.

Appendix

According to the Monin–Obukhov similarity theory (MOST), the aerodynamic resistance between the heights z_1 and z_2 is defined as

$$R_a(z_1,z_2) = \int_{z_1}^{z_2} \frac{dz}{K(z)} \quad (A1)$$

where the vertical eddy diffusivity (turbulent exchange coefficient) K is

$$K(z) = \frac{\kappa u_*(z-d)}{\varphi(z)} \quad (A2)$$

where κ is the von Kármán constant, u_* is friction velocity and d is zero-plane displacement height; φ is the dimensionless profile function, which only depends on the dimensionless stability,

$$\zeta \equiv \frac{z-d}{L} \quad (A3)$$

where L is the Obukhov length. Introducing ζ by variable transformation [and denoting $\zeta_i \equiv (z_i-d)/L$ $(i=1, 2)$], we can write

$$R_a(z_1,z_2) = \frac{1}{\kappa u_*}\int_{\zeta_1}^{\zeta_2} \frac{\varphi(\zeta)}{\zeta} d\zeta \quad (A4)$$

and further

$$\kappa u_* R_a(z_1,z_2) = \int_{\zeta_1}^{\zeta_2} \left(\frac{1}{\zeta} - \frac{1-\varphi(\zeta)}{\zeta}\right) d\zeta \quad (A5)$$

Evaluating this integral yields the general form

$$\kappa u_* R_a(z_1,z_2) = \ln\frac{z_2-d}{z_1-d} - \Psi(\zeta_1,\zeta_2) \quad (A6)$$

where we have defined the dimensionless diabatic correction function corresponding to φ as

$$\Psi(\zeta_1,\zeta_2) \equiv \int_{\zeta_1}^{\zeta_2} \frac{1-\varphi(\zeta)}{\zeta} d\zeta \quad (A7)$$

The above equations represent the standard MOST (e.g. Garratt, 1992). This formalism can be generalised for the enhanced eddy diffusivity within the roughness sublayer (RSL) as follows. For the aerodynamic resistance modified for the RSL we write

$$R_a^*(z_1,z_2) = \frac{1}{\kappa u_*}\int_{z_1}^{z_2} \frac{\varphi^*(z)}{z-d} dz, \quad z_1 \le z_2 \le z^* \quad (A8)$$

where φ^* is the dimensionless profile function in the RSL and z^* is the RSL height.

Analogously to Eqs. (A6) and (A7) we can define a general form

$$\kappa u_* R_a^*(z_1,z_2) = \ln\frac{z_2-d}{z_1-d} - \Psi^*(\zeta_1,\zeta_2) \quad (A9)$$

with

$$\Psi^*(\zeta_1,\zeta_2) \equiv \int_{\zeta_1}^{\zeta_2} \frac{1-\varphi^*(\zeta)}{\zeta} d\zeta, \quad \zeta_1 \le \zeta_2 \le \zeta^* \quad (A10)$$

where $\zeta^* \equiv (z^*-d)/L$.

By this definition, Ψ^* represents both stability and RSL effects. Hence, while the logarithmic part of R_a in Eq. (A6) represents the neutral stability ($\Psi = 0$, if $L^{-1}=0$), in a general case this is not true for R_a^* in Eq. (A9).

Observations show that

$$\varphi(\zeta) = \begin{cases} (1-\beta\zeta)^{-1/2}, & \zeta < 0 \\ 1+\gamma\zeta, & \zeta \ge 0 \end{cases} \quad (A11)$$

where β and γ are constants (Garratt, 1992). [$\beta = 16$ and $\gamma = 5$ are used in the EMEP model (Simpson et al., 2003a).] The corresponding diabatic correction function is

$$\Psi(\zeta_1,\zeta_2) = \begin{cases} 2\ln\dfrac{1+\varphi(\zeta_2)^{-1}}{1+\varphi(\zeta_1)^{-1}}, & L^{-1} < 0 \\ -\gamma(\zeta_2-\zeta_1), & L^{-1} \ge 0 \end{cases} \quad (A12)$$

For the RSL no established similarity theory or universal profile function exists, but the RSL effects are commonly expressed by a multiplicative factor representing the enhancement of eddy diffusivity, $\epsilon(z)$. The corresponding dimensionless profile function in the RSL is then

$$\varphi^*(z) = \frac{\varphi(z)}{\epsilon(z)} \quad (A13)$$

We employ the enhancement factor proposed by Raupach et al. (1980), Cellier and Brunet (1992) and Mölder et al. (1999),

$$\epsilon(z) = \frac{z^*-d}{z-d}, \quad d \le z \le z^* \quad (A14)$$

Inserting Eqs. (A13) and (A14) into Eq. (A10), we obtain

$$\Psi^*(\zeta_1,\zeta_2) = \int_{\zeta_1}^{\zeta_2} \frac{d\zeta}{\zeta} - \frac{1}{\zeta^*}\int_{\zeta_1}^{\zeta_2} \varphi(\zeta) d\zeta \quad (A15)$$

which with Eq. (A11) yields

$$\Psi^*(\zeta_1,\zeta_2) = \begin{cases} \ln\dfrac{\zeta_2}{\zeta_1} + \dfrac{2}{\beta\zeta^*}\left(\varphi(\zeta_2)^{-1} - \varphi(\zeta_1)^{-1}\right), & L^{-1} < 0 \\ \ln\dfrac{\zeta_2}{\zeta_1} - \dfrac{1}{\zeta^*}\left[\zeta_2-\zeta_1+\dfrac{\gamma}{2}\left(\zeta_2^2-\zeta_1^2\right)\right], & L^{-1} > 0 \end{cases} \quad (A16)$$

Thus we obtain from Eq. (A9)

$$R_a^*(z_1,z_2) = \begin{cases} \dfrac{2}{\kappa u_* \beta \zeta^*}\left(\varphi(\zeta_1)^{-1} - \varphi(\zeta_2)^{-1}\right), & L^{-1} < 0 \\ \dfrac{1}{\kappa u_* \zeta^*}\left[\zeta_2 - \zeta_1 + \dfrac{\gamma}{2}\left(\zeta_2^2 - \zeta_1^2\right)\right], & L^{-1} > 0 \end{cases} \quad \text{(A17)}$$

In the neutral limit Eq. (A16) converges to

$$\Psi^*(\zeta_1,\zeta_2) = \ln\frac{z_2-d}{z_1-d} - \frac{z_2-z_1}{z^*-d}, \quad L^{-1} = 0 \quad \text{(A18)}$$

and Eq. (A17) to

$$R_a^*(z_1,z_2) = \frac{z_2-z_1}{\kappa u_*(z^*-d)}, \quad L^{-1} = 0 \quad \text{(A19)}$$

References

Affre, C., Carrara, A., Lefebre, F., Druilhet, A., Fontan, J., Lopez, A., 1999. Aircraft measurements of ozone turbulent flux in the atmospheric boundary layer. Atmospheric Environment 33, 1561–1574.

Ashmore, M., Emberson, L., Karlsson, P.E., Pleijel, H., 2004. Introduction for ozone deposition special issue. Atmospheric Environment 38, 2211–2212.

Benedictow, A., 2003. Documentation and Verification of the 1999 PARLAM-PS Meteorological Fields Used as Input for Eulerian EMEP Model. Research Note 111. Norwegian Meteorological Institute, Oslo.

Bosveld, F.C., 1997. Derivation of fluxes from profiles over a moderately homogeneous forest. Boundary-Layer Meteorology 84, 289–327.

Brutsaert, W., 1982. Evaporation into the Atmosphere. Reidel, Dordrecht, p. 299.

CEC, 2005. Annex to The Communication on Thematic Strategy on Air Pollution and The Directive on "Ambient Air Quality and Cleaner Air for Europe", Impact Assessment. Commission Staff Working Paper SEC(2005) 1133, p. 170. Commission of the European Communities (CEC), Brussels. Available from: <http://ec.europa.eu/environment/archives/cafe>.

Cellier, P., 1986. On the validity of flux–gradient relationships above very rough surfaces. Boundary-Layer Meteorology 36, 417–419.

Cellier, P., Brunet, Y., 1992. Flux–gradient relationships above tall plant canopies. Agricultural and Forest Meteorology 58, 93–117.

Chen Fazu, Schwerdtfeger, P., 1989. Flux-gradient relationships for momentum and heat over a rough natural surface. Quarterly Journal of the Royal Meteorological Society 115, 335–351.

Dellwik, E., Jensen, N.O., 2005. Flux–profile relationships over a fetch limited beech forest. Boundary-Layer Meteorology 115, 179–204.

Dias, N.L., Brutsaert, W., 1996. Similarity of scalars under stable conditions. Boundary-Layer Meteorology 80, 355–373.

Dorsey, J.R., Duyzer, J.H., Gallagher, M.W., Coe, H., Pilegaard, K., Weststrate, J.H., Jensen, N.O., Walton, S., 2004. Oxidized nitrogen and ozone interaction with forests, I: experimental observations and analysis with Douglas fir. Quarterly Journal of the Royal Meteorological Society 130, 1941–1955.

Droppo Jr., J.G., 1985. Concurrent measurements of ozone dry deposition using eddy correlation and profile flux methods. Journal of Geophysical Research 90, 2111–2118.

Duyzer, J., Weststrate, H., 1995. The use of the gradient method to monitor trace gas fluxes over forest: flux-profile functions for ozone and heat. In: Heij, G.J., Erisman, J.W. (Eds.), Acid Rain Research: Do We Have Enough Answers. Studies in Environmental Science, vol. 64. Elsevier, Amsterdam, pp. 21–30.

Emberson, L.D., Simpson, D., Tuovinen, J.-P., Ashmore, M.R., Cambridge, H. M., 2000. Towards a Model of Ozone Deposition and Stomatal Uptake Over Europe. EMEP/MSC-W Note 6/2000, p. 58. Norwegian Meteorological Institute, Oslo. Available from: <www.emep.int>.

Erisman, J.W., Vermeulen, A., Hensen, A., Flechard, C., Dämmgen, U., Fowler, D., Sutton, M., Grünhage, L., Tuovinen, J.-P., 2005. Monitoring and modelling of biosphere/atmosphere exchange of gases and aerosols in Europe. Environmental Pollution 133, 403–413.

Foken, T., 2006. 50 years of the Monin–Obukhov similarity theory. Boundary-Layer Meteorology 119, 431–447.

Garratt, J.R., 1980. Surface influence upon vertical profiles in the atmospheric near-surface layer. Quarterly Journal of the Royal Meteorological Society 106, 803–819.

Garratt, J.R., 1992. The Atmospheric Boundary Layer. Cambridge University Press, Cambridge, UK, p. 316.

Goldstein, A.H., McKay, M., Kurpius, M.R., Schade, G.W., Lee, A., Holzinger, R., Rasmussen, R.A., 2004. Forest thinning experiment confirms ozone deposition to forest canopy is dominated by reaction with biogenic VOCs. Geophysical Research Letters 31, L22106.

Hayes, F., Mills, G., Harmens, H., Norris, D., 2007. Evidence of Widespread Ozone Damage to Vegetation in Europe (1990–2006). Programme Coordinating Centre for the ICP Vegetation, Centre for Ecology and Hydrology, Bangor, UK, p. 60. Available from: <icpvegetation.ceh.ac.uk>.

Hicks, B.B., Baldocchi, D.D., Meyers, T.P., Hosker Jr., R.P., Matt, D.R., 1987. A preliminary multiple resistance routine for deriving dry deposition velocities from measured quantities. Water Air and Soil Pollution 36, 311–330.

Hill, R.J., 1989. Implications of the Monin–Obukhov similarity theory for scalar quantities. Journal of Atmospheric Sciences 46, 2236–2244.

Hjellbrekke, A.-G., Solberg, S., 2002. Ozone Measurements 2000, EMEP/CCC Report 5/2002, p. 90. Norwegian Institute for Air Research, Kjeller. Available from: <www.emep.int>.

Högström, U., Bergström, H., Smedman, A.-S., Halldin, S., Lindroth, A., 1989. Turbulent exchange above a pine forest, I: fluxes and gradients. Boundary-Layer Meteorology 49, 197–217.

Lamaud, E., Irvine, M., 2006. Temperature–humidity dissimilarity and heat-to-water-vapour transport efficiency above and within a pine forest canopy: the role of the Bowen ratio. Boundary-Layer Meteorology 120, 87–109.

Mammarella, I., Dellwik, E., Jensen, N.O., 2008. Turbulence spectra, shear stress and turbulent kinetic energy budgets above two beech forest sites in Denmark. Tellus 60B, 179–187.

Mills, G. (Ed.), 2004. Mapping Critical Levels for Vegetation, Manual on Methodologies and Criteria for Modelling and Mapping Critical Loads & Levels and Air Pollution Effects, Risks and Trends. UNECE Convention on Long-range Transboundary Air Pollution, Geneva, p. 52 (Chapter 3). Available from: <www.icpmapping.org>.

Mills, G. (Ed.), 2007. Mapping Critical Levels for Vegetation, Mapping Manual Revision. UNECE Convention on Long-range Transboundary Air Pollution, Geneva, p. 74. Available from: <www.icpmapping.org>.

Mölder, M., Grelle, A., Lindroth, A., Halldin, S., 1999. Flux-profile relationships over a boreal forest – roughness sublayer corrections. Agricultural and Forest Meteorology 98–99, 645–658.

Nakamura, R., Mahrt, L., 2001. Similarity theory for local and spatially averaged momentum fluxes. Agricultural and Forest Meteorology 108, 265–279.

Neirynck, J., Kowalski, A.S., Carrara, A., Ceulemans, R., 2005. Driving forces for ammonia fluxes over mixed forest subjected to high deposition loads. Atmospheric Environment 39, 5013–5024.

Paoletti, E., Manning, W.J., 2007. Towards a biologically significant and usable standard for ozone that will also protect plants. Environmental Pollution 150, 85–95.

Pearson Jr., R.J., Oncley, S.P., Delany, A.C., 1998. A scalar similarity study on surface layer ozone measurements over cotton during the California ozone deposition experiment. Journal of Geophysical Research 103, 18919–18926.

Rannik, Ü., 1998. On the surface layer similarity at a complex forest site. Journal of Geophysical Research 103, 8685–8697.

Rannik, Ü., Keronen, P., Hari, P., Vesala, T., 2004. Estimation of forest–atmosphere CO_2 exchange by eddy covariance and profile techniques. Agricultural and Forest Meteorology 126, 141–155.

Raupach, M.R., 1979. Anomalies in flux-gradient relationships over forest. Boundary-Layer Meteorology 16, 467–486.

Raupach, M.R., Thom, A.S., Edwards, I., 1980. A wind-tunnel study of turbulent flow close to regularly arrayed rough surfaces. Boundary-Layer Meteorology 18, 373–397.

Raupach, M.R., 1995. Vegetation–atmosphere interaction and surface conductance at leaf, canopy and regional scales. Agricultural and Forest Meteorology 73, 151–179.

Raupach, M.R., Finnigan, J.J., Brunet, Y., 1996. Coherent eddies and turbulence in vegetations canopies: the mixing-layer analogy. Boundary-Layer Meteorology 78, 351–382.

Ruppert, J., Thomas, C., Foken, T., 2006. Scalar similarity for relaxed eddy accumulation methods. Boundary-Layer Meteorology 120, 39–63.

Schween, J.H., Zelger, M., Wichura, B., Foken, T., Dlugi, R., 1997. Profiles and fluxes of micrometeorological parameters above and within the Mediterranean forest at Castelporziano. Atmospheric Environment 31 (S1), 185–198.

Simpson, D., Fagerli, H., Jonson, J.E., Tsyro, S., Wind, P., Tuovinen, J.-P., 2003a. Transboundary Acidification, Eutrophication and Ground Level

Ozone in Europe, Part I. Unified EMEP Model Description. EMEP Status Report 1/2003, p. 74 + App. Norwegian Meteorological Institute, Oslo. Available from: <www.emep.int>.

Simpson, D., Tuovinen, J.-P., Emberson, L., Ashmore, M., 2003b. Characteristics of an ozone deposition module II: sensitivity analysis. Water Air and Soil Pollution 143, 123–137.

Simpson, D., Emberson, L., 2006. Ozone fluxes – updates. In: Transboundary Acidification, Eutrophication and Ground Level Ozone in Europe from 1990 to 2004 in Support for the Review of the Gothenburg Protocol, EMEP Report 1/2006. Norwegian Meteorological Institute, Oslo, pp. 63–79. Available from: <www.emep.int>.

Simpson, D., Ashmore, M., Emberson, L., Tuovinen, J.-P., 2007. A comparison of two different approaches for mapping potential ozone damage to vegetation. A model study. Environmental Pollution 146, 715–725.

Simpson, I.J., Thurtell, G.W., Neumann, H.H., den Hartog, G., Edwards, G.C., 1998. The validity of similarity theory in the roughness sublayer above forests. Boundary-Layer Meteorology 87, 69–99.

Sliggers, S., Kakebeeke, W. (Eds.), 2004. Clearing the Air, 25 Years of the Convention on Long-Range Transboundary Air Pollution. United Nations, Economic Commission for Europe, Geneva, p. 168. Available from: <http://www.unece.org/env/lrtap>.

Sofiev, M., Tuovinen, J.-P., 2001. Factors determining the robustness of AOT40 and other ozone exposure indices. Atmospheric Environment 35, 3521–3528.

Thom, A.S., Stewart, J.B., Oliver, H.R., Gash, J.H.C., 1975. Comparison of aerodynamic and energy budget estimates of fluxes over a pine forest. Quarterly Journal of the Royal Meteorological Society 101, 93–105.

Tuovinen, J.-P., 2000. Assessing vegetation exposure to ozone: properties of the AOT40 index and modifications by deposition modelling. Environmental Pollution 109, 361–372.

Tuovinen, J.-P., Ashmore, M., Emberson, L., Simpson, D., 2004. Testing and improving the EMEP ozone deposition module. Atmospheric Environment 38, 2373–2385.

Tuovinen, J.-P., Simpson, D., Emberson, L., Ashmore, M., Gerosa, G., 2007. Robustness of modelled ozone exposures and doses. Environmental Pollution 146, 578–586.

Verhoef, A., McNaughton, K.G., Jacobs, A.F.G., 1997. A parameterization of momentum roughness length and displacement height for a wide range of canopy densities. Hydrology and Earth System Sciences 1, 81–91.

Wesely, M.L., 1988. Use of variance techniques to measure dry air-surface exchange rates. Boundary-Layer Meteorology 44, 13–31.

Williams, C.A., Scanlon, T.M., Albertson, J.D., 2007. Influence of surface heterogeneity on scalar dissimilarity in the roughness sublayer. Boundary-Layer Meteorology 122, 149–165.